Electronic structure and charge-density wave formation in $LaTe_{1.95}$ and $CeTe_{2.00}$

K. Y. Shin,[1] V. Brouet,[2] N. Ru,[1] Z. X. Shen,[1] and I. R. Fisher[1,*]
[1]*Geballe Laboratory for Advanced Materials and Department of Applied Physics, Stanford University, Stanford, California 94305, USA*
[2]*Laboratoire de Physique des Solides, Universite Paris-Sud, Bat 510, UMR 8502, 91405 Orsay, France*
(Received 30 May 2005; published 24 August 2005)

Results are presented of complementary measurements that probe the electronic structure and charge-density wave (CDW) modulation in the quasi-two-dimensional compounds $LaTe_{1.95}$ and $CeTe_2$. Transmission electron micrographs show that the modulation wave vectors associated with the CDW are different for the two materials, and in both cases are incommensurate with the underlying lattice. These wave vectors are shown to correspond to nesting features of a simplified model of the Fermi surface. Angle-resolved photoemission spectroscopy is used to reveal the electronic structure and Fermi-surface topology in the CDW state. The data indicate a large CDW gap that varies in magnitude around the Fermi surface somewhat differently for the two compounds. Differences in the volume of the original Fermi surface are related to the doping effect of Te vacancies. Heat-capacity measurements at low temperatures indicate a very small electronic density of states, consistent with the electrical resistivity, which appears to be semiconducting or semimetallic.

DOI: 10.1103/PhysRevB.72.085132 PACS number(s): 71.18.+y, 71.45.Lr, 72.15.−v, 79.60.−i

I. INTRODUCTION

$RTe_{2-\delta}$ (R=La,Ce; δ=0∼0.18) compounds have attracted recent attention due to their effective low dimensionality. The materials play host to a charge-density wave[1,2] (CDW) and can be described in terms of a modulated Cu_2Sb-type structure ($P4/nmm$) based on alternating layers of square-planar Te sheets and a corrugated RTe slab (Fig. 1). Band-structure calculations for the stoichiometric material indicate a strongly anisotropic Fermi surface (FS) of mostly Te 5p character with minimal c-axis dispersion, large regions of which are nested.[3,4] A substantial anisotropy in the electrical resitivity confirms the quasi-two-dimensional character of the charge carriers,[5–7] and a superlattice modulation of the average structure has been observed via transmission electron microscopy (TEM)[1] and x-ray diffraction.[8,9] DiMasi *et al.* previously showed that the modulation wave vectors can be tuned by Sb substitution in $LaTe_{2-x}Sb_x$, and that these wave vectors can be understood in terms of optimal nesting of a Fermi surface derived from simple tight-binding arguments.[1] These observations essentially establish the lattice modulation in RTe_2 as a CDW, driven by an electronic instability of the Fermi surface. More recently, tunneling measurements on $RTe_{2-\delta}$ for both R=La and Ce clearly reveal a well-developed gap, further supporting the idea of CDW formation.[2] Here, the Ce is trivalent and the 4f states do not appear to contribute to the Fermi surface,[10] ordering antiferromagnetically below 6 K.[11,12] No clear electronic phase transitions are observed below 300 K, and the material appears to be deep in the CDW state even at room temperature, similar to the related bilayer material RTe_3 (R=Y,La-Sm,Gd-Er).[13–15] The structural and electronic simplicity of RTe_2 and RTe_3, combined with the large size of the CDW gap, makes these particularly attractive materials for studying the effect of CDW formation on the electronic structure of layered materials. In particular, angle-resolved photoemission spectroscopy (ARPES) has enabled direct measurement of the electronic structure in the CDW state of RTe_3,[14,15] and we show here that it is also possible in RTe_2.

$RTe_{2-\delta}$ compounds have a substantial width of formation[16] corresponding to a tendency toward significant Te vacancies on the Te(1) square planar site.[17,18] In contrast, the related bilayer rare-earth tellurides RTe_3 form as stoichiometric compounds without significant Te deficiency.[19] Reports of transport properties for $RTe_{2-\delta}$ (R=La,Ce; δ=0∼0.18) vary widely,[5,7] and presumably can be related to differences in Te deficiency between samples produced via different crystal-growth techniques. Recently, pressure-induced superconductivity at T_c=2.7 K has been reported in nonstoichiometic $CeTe_{1.82}$.[20] These data indicate a possible coexistence of the CDW and superconducting and antiferromagnetic phases at low temperature, although the origin of the superconductivity is not clear. Similar high-pressure measurements have not been made for other rare earths in this family of compounds, but the authors report that the superconductivity in $CeTe_{2-\delta}$ is very sensitive to δ,[20] suggestive of an intimate link to the electronic structure and CDW modulation. In an attempt to explain the mechanism of the superconductivity, a band-structure calculation has been performed which models the effects of Te deficiency and assumes specific commensurate distortions of the host

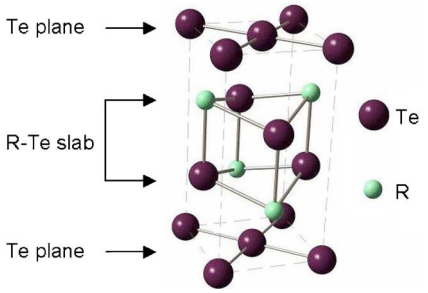

FIG. 1. (Color online) Schematic diagram showing the average (unmodulated) crystal structure of RTe_2, which has the Cu_2Sb-type structure ($P4/nmm$). Dashed lines show the unit cell. The c axis is vertical.

lattice,[21] although as we argue later, these assumptions may be too simplistic.

In this paper, we describe the results of TEM, ARPES, heat-capacity, and resistivity measurements of single crystals of $CeTe_2$ and $LaTe_{1.95}$. The measurements provide complementary information about the lattice modulation and the electronic structure and Fermi-surface topology for the two compounds. We have prepared the materials in single-crystal form, using an alternative self-flux technique, which lends itself to minimizing Te deficiency while reducing the risk of contamination by not using a separate flux or transport agent. The Ce compound is stoichiometric to within the resolution of our compositional analysis, but the La compound is found to have a small Te deficiency that is barely measurable within the resolution of the microprobe technique. Neither material exhibits a simple commensurate CDW corresponding to doubling of the unit cell (although both show wave vectors very close to this), but rather have a complex series of incommensurate wave vectors that are different from published data for crystals grown by alternative techniques. The CDW distortion is different for the two compounds, which is also reflected in a more dramatic difference in the electronic structure as revealed by the ARPES measurements. Our results indicate that subtle differences, such as the choice of rare earth or relatively minor changes in Te deficiency and band filling, can substantially affect the superlattice modulation and electronic structure of $RTe_{2-\delta}$. These results imply that understanding the pressure-induced superconductivity in $CeTe_{1.82}$ will require more than a simple extrapolation from the electronic structure and CDW modulation of the stoichiometric compounds.

II. SAMPLE PREPARATION

Previously, single crystals of $RTe_{2-\delta}$ have been grown via chemical vapor transport,[8,9] from an alkali-halide flux,[1] via mineralization of a nominally stoichiometric binary mixture of elements,[7] and via a high-temperature Bridgman method.[5,11] Here we describe a related self-flux technique that we favor since it produces crystals with a very small Te deficiency without the use of a third-element flux or a chemical transport agent. Furthermore, by using a hot-decanting technique to remove the flux before it solidifies, we are also able to minimize strain in the resulting crystals.

With reference to the binary phase diagrams of Ce-Te and La-Te,[16] it is clear that single crystals of both RTe_3 and RTe_2 (R=La,Ce) can be grown from a binary melt. Our experiments indicate that the exact position of the liquidus in the published phase diagrams is not entirely accurate, but nevertheless it is a good starting point. Previously, we have prepared single crystals of $CeTe_3$ using this technique, slowly cooling a Te-rich melt.[14] The growth of RTe_2 requires a greater relative concentration of the rare-earth element, and substantially higher temperatures, but is otherwise very similar. Elements in the molar ratio from $Ce_{0.14}Te_{0.86}$ to $Ce_{0.18}Te_{0.82}$ and from $La_{0.15}Te_{0.85}$ to $La_{0.18}Te_{0.82}$ were put into alumina crucibles and vacuum sealed in quartz tubes. The mixtures were heated to 1150 °C and slowly cooled over a period of 3–5 days to end temperatures in the range of 900–1060 °C. Such high temperatures (Te boils at around 1000 °C at 1 atm) are possible for this growth because the substantial fraction of rare-earth element reduces the Te vapor pressure, but nevertheless care must be taken that the quartz tubes are well sealed. Resulting crystals were separated from the remaining melt by decanting in a centrifuge. The crystals were shaped in the form of dark, shiny, somewhat brittle platelets, with dimensions up to $10\times10\times1$ mm^3, with the c axis perpendicular to the plane of the crystal plates.

We have made a particular effort to produce stoichiometric, or as close to stoichiometric as possible, single crystals of $RTe_{2-\delta}$. With reference again to the binary phase diagrams,[16] a smaller Te deficiency δ is possible for melts that have a larger Te content, requiring lower growth temperatures. Composition of the resulting crystals was determined by electron microprobe analysis using elemental standards, and showed that we are able to produce stoichiometic crystals of $CeTe_{2.00}$ by this technique, with an uncertainty of ±0.03 in the Te content. However, all attempts to produce stoichiometic $LaTe_2$ failed, and the highest composition achieved by this technique was $LaTe_{1.95}$, which is only just substoichiometric within the resolution of our measurements. Published data for crystals grown via the mineralization technique of Ref. 7 indicate a Te deficiency of $\delta=0.15-0.18$. In comparison, the self-flux technique produces crystals with a much smaller Te deficiency $\delta=0.00$ (R=Ce)–0.05 (R=La). The Bridgman technique described in Refs. 5 and 11 reportedly produces stoichiometric crystals, although the high temperature used for this growth implies a larger Te deficiency than the lower temperatures that we employ. According to published work, both the alkali-halide flux[1] and chemical vapor transport[8,9] techniques also produce crystals with a very small Te deficiency, although in general we favor a self-flux since it minimizes the possibility of contamination from additional elements.

III. EXPERIMENTAL METHODS

For transmission electron microscopy (TEM), thin crystals of $LaTe_{1.95}$ and $CeTe_2$ with thickness less then 30 μm were carefully selected and mounted on copper grids. To achieve optimal thickness for the measurement, a small hole was made in the middle of the crystals by ion-milling in vacuum for 2 h. The crystals were illuminated on the edge of the hole and selected area diffraction patterns (SADPs) were obtained using a Philips CM20 FEG-TEM operating at 200 kV in vacuum at room temperature. In order to observe the superlattice reflections from the periodic lattice modulation in the *ab* plane, the electron beam was aligned normal to the *ab* plane in the [001] zone axis.

ARPES data were collected at 25 K on Beam Line 10 of the Advanced Light Source, with the beam polarization nearly perpendicular to the sample surface, photon energy between 30 and 50 eV, and an energy resolution of ~20 meV. RTe_2 does not cleave as easily as RTe_3. In RTe_3, the natural cleavage plane is between Te layers, which reveals the Te sheets, whereas in RTe_2 it is most likely between Te layers and the RTe slab, giving only a 50% chance to

observe directly the Te sheets. Samples were glued with Torr-Seal epoxy and electrically connected to the ground by graphite. No electrical charging of the sample surface occurred in these conditions during the measurement.

The heat capacity of the single-crystal samples was measured using a relaxation-time technique. Crystals with a mass of approximately 5–10 mg were prepared with a flat surface for good thermal contact with the sample platform. Data for $LaTe_{1.95}$ were used to obtain estimates of the electronic contribution to the heat capacity. Similar measurements were also made for $LaTe_3$ single crystals for comparison.

The electrical resistivity was measured using geometric bars cut and cleaved from the larger as-grown crystals. Electrical contact was made using Dupont 4929 silver epoxy on sputtered or evaporated gold pads, with typical contact resistances of 1.0–2.5 Ω. Resistivity measurements were made at 16 Hz and with current densities of approximately 0.03 A/cm^2. In-plane measurements were made for arbitrary current directions in the *ab* plane, using a standard four-point contact geometry. The *c*-axis resistivity was measured using a modified Montgomery geometry, with one current and one voltage contact on the top face of the platelike crystal, and the other voltage and current contacts on the bottom face. Several measurements were made for crystals from each growth batch.

IV. TEM

SADPs taken at room temperature for $LaTe_{1.95}$ and $CeTe_2$ single crystals are shown in Fig. 2. The undistorted tetragonal $P4/nmm$ structure produces strong $(hk0)$ peaks in reciprocal space where $h+k$=even and no peaks where $h+k$=odd.

In-plane tetragonal lattice parameters obtained from the observed patterns are $a=4.55\pm0.02$ Å for $LaTe_2$ and $a=4.52\pm0.02$ Å for $CeTe_2$, which agree within the uncertainty with published values of $a=4.52$ Å for $LaTe_2$ (Ref. 1) and $a=4.47$ Å for $CeTe_2$ (Ref. 12) obtained from x-ray diffraction measurements. Both diffraction patterns shown in Fig. 2 also have faint spots at the $h+k$=odd forbidden-peak positions, the presence of which have previously been attributed to the combination of sample bending and/or stacking disorder.[13] In the case of $LaTe_{1.95}$, these additional spots also appear to be slightly split, but the origin of this effect is unclear.

Additional superlattice peaks in the SADPs for both compounds indicate the presence of a modulation from the simple Cu_2Sb structure. These patterns were reproduced for several crystals of each rare-earth element. In both cases, the diffraction patterns exhibit a fourfold rotational symmetry, rather than the simpler twofold symmetry that was previously observed for nominally stoichiometric $LaTe_2$.[1] No measurements showed a simple twofold symmetry, including measurements of different sections of the same crystals, which leads us to think that this is an intrinsic symmetry of the material, although we cannot completely rule out the possibility of some kind of microtwinning. Positions of the various satellite peaks in the first quadrant are listed in Table I for both compounds ($a^*=2\pi/a$, etc.). Those in other quarters are mapped by reflection and the fourfold symmetry of the lattice.

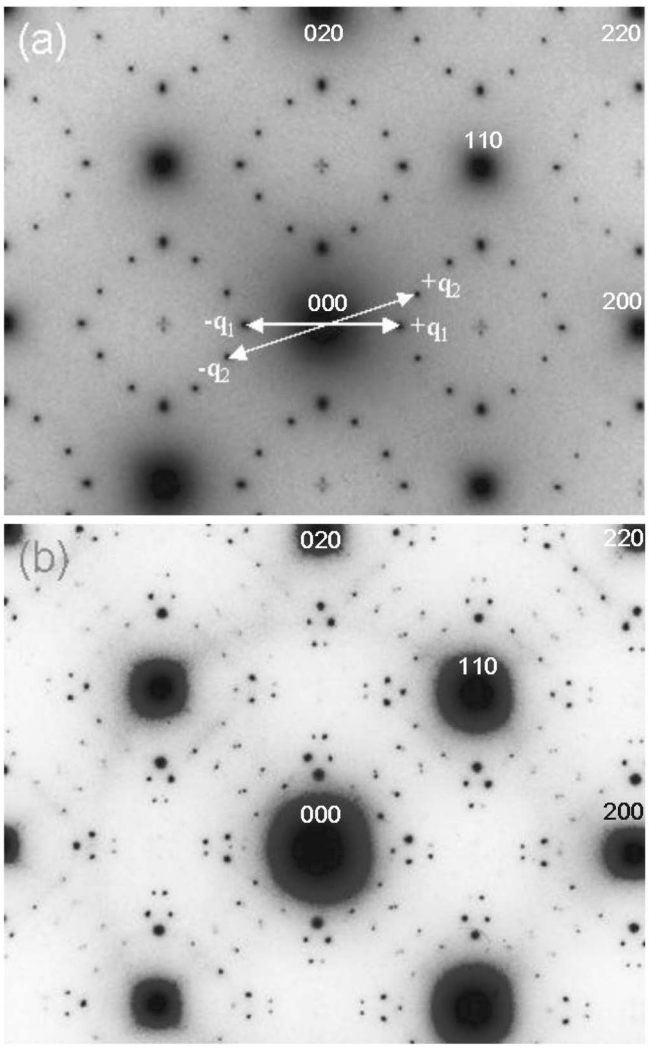

FIG. 2. Selected area diffraction patterns of (a) $LaTe_{1.95}$ and (b) $CeTe_2$ in the [001] zone axis. The most intense diffraction peaks correspond to $h+k$=even.

$LaTe_{1.95}$ has the simpler diffraction pattern of the two compounds, and the lattice modulation can be characterized by two independent wave vectors, after taking into account

TABLE I. CDW wave vectors $\vec{q}=\alpha\vec{a}^*+\beta\vec{b}^*$, α, and β in the first quadrant formed by (000), (100), and (010).

Crystal	α	β
$LaTe_{1.95}$	0.484±0.002	0.000±0.005
	0.601±0.002	0.201±0.002
$CeTe_{2.00}$	0.473±0.003	0.0000±0.003
	0.572±0.002	0.067±0.003
	0.715±0.002	0.035±0.003
	0.396±0.002	0.219±0.002
	0.487±0.002	0.354±0.003

the fourfold symmetry, neither of which can be easily related to the periodicity of the underlying lattice. One of the two vectors is close but not equal to the commensurate wave vector $0.5a^*$, which would correspond to doubling the unit cell, and that was previously observed for the nominally stoichiometric $LaTe_2$ crystals[1] described earlier. The other vector was not previously observed at all (although we note that $LaTe_{1.8}Sb_{0.2}$ was found to have a modulation wave vector $q=0.672a^*+0.078b^*$).[1] The fourfold symmetry and additional modulation vectors may simply reflect the difference in Te content of crystals grown by the two techniques, or it might be related to the synthesis conditions themselves (which can affect strain, stacking order, etc.).

In contrast to $LaTe_{1.95}$, the diffraction pattern for $CeTe_2$ is much more complex. As for $LaTe_{1.95}$, one of the observed wave vectors is close but not equal to the commensurate case of $0.5a^*$. The difference between the diffraction patterns of $CeTe_2$ and $LaTe_{1.95}$ may be due to the difference in Te deficiency, or might be related to the subtle Lanthanide contraction. Whatever the cause, we can anticipate that the electronic structure of the two compounds will be somewhat different.

Previously, DiMasi and co-workers related the commensurate $0.5a^*$ lattice modulation that they observed for $LaTe_2$ to a nesting condition of a model Fermi surface constructed using a tight-binding approach for square Te planes.[1] They showed that tuning the band filling in this model resulted in changes in the nesting wave vector, and indeed observed changes in the modulation wave vector for Sb-doped single crystals. In a similar vein, we use the same model to illustrate that more complex lattice modulations are possible for this structure, and that these are not too dissimilar to the modulation vectors that we observe for $CeTe_2$ and $LaTe_{1.95}$.

We do this by calculating the Lindhart susceptibility $\chi(q)$ for the same toy model of a single square-planar Te sheet, illustrated in Fig. 3(a). We choose values of $t_\parallel$ and $t_\perp$ that give results that closely appoximate more careful band calculations by Kikuchi,[4] but we neglect the effect of hybridization between the p_x and p_y orbitals. The resulting tight-binding band structure and Fermi surface are shown in Figs. 3(b) and 3(c) for a band-filling corresponding to stoichiometric composition ($\delta=0$). Comparison with the results of full band calculations for undistorted $LaTe_2$[3,4] show that this model, although extremely simplistic, does in fact capture the essence of the electronic structure of RTe_2, reflecting the simplicity of material. The Lindhart susceptibility calculated by summing over all bands and all energies for this model is shown as a color-scale plot in Fig. 4(a). We have used a band filling that closely approximates the observed Fermi surface for $LaTe_{1.95}$ (corresponding to a Fermi energy $E_F=3.1$ eV; see Sec. V), consistent with the small Te deficiency that acts to donate electrons. In the same figure, we show the observed lattice modulation wave vectors for this compound taken from Table I. It is clear from Fig. 4(a) that $\chi(q)$ does not have a simple single peak corresponding to $q=0.5a^*$, but rather has a tendency to have a range of maxima corresponding to nesting of different regions of the Fermi surface. Even so, the observed lattice modulation vectors for $LaTe_{1.95}$ certainly lie in regions of Fig. 4(a) for which $\chi(q)$ has a large value. For comparison, in Fig. 4(b) we show the Fermi surface corresponding to this particular band filling together with a CDW replica that has been translated by $q_{CDW}=(0.601a^*,0.201a^*)$, one of the two wave vectors observed for $LaTe_{1.95}$. As can be seen, this wave vector almost nests an extended region of the model Fermi surface, which would presumably be the driving force for the resulting lattice modulation. Although this model clearly lacks a number of details that can be very significant in determining finer behavior of $\chi(q)$, the calculation is useful in that it suggests that this quantity does not have a simple single peak, and that relatively subtle effects may therefore favor one wave vector over another. This is in direct contrast to RTe_3, for which a

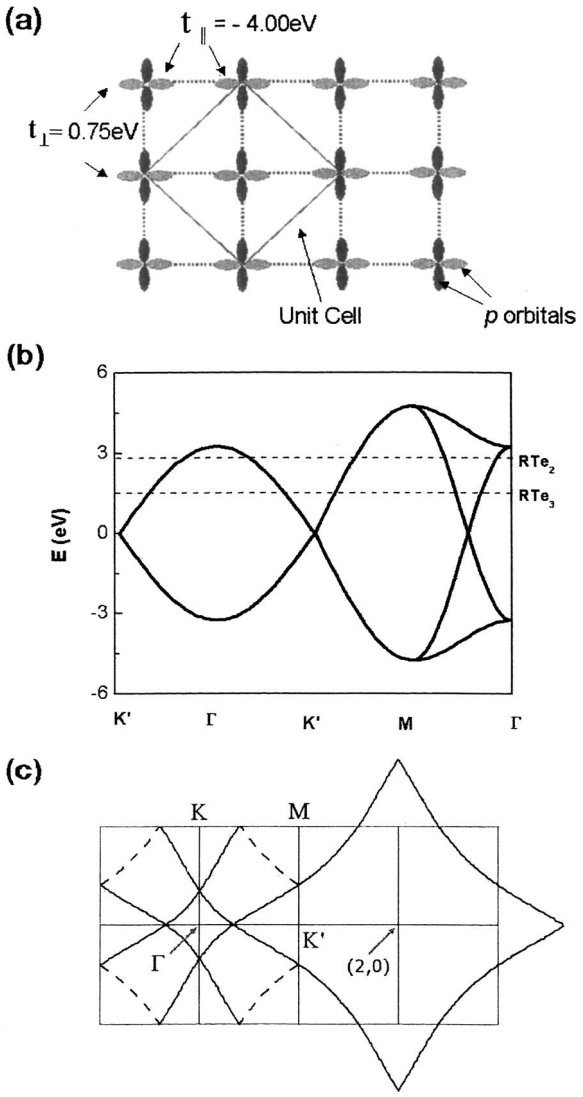

FIG. 3. (a) Real-space representation of a square-planar Te sheet, indicating p_x and p_y orbitals used in the tight-binding model calculation. (b) The band structure for the model, showing band filling corresponding to RTe_2 and RTe_3. (c) The resulting Fermi surface for RTe_2, neglecting hybridization between p_x and p_y orbitals. The solid lines indicate bands in the extended-zone scheme and show sections that we identify as the inner and outer FS, centered at Γ and (2,0), respectively. Dashed lines represent the bands folded into the reduced zone according to the periodicity of the unit cell, as shown in (a).

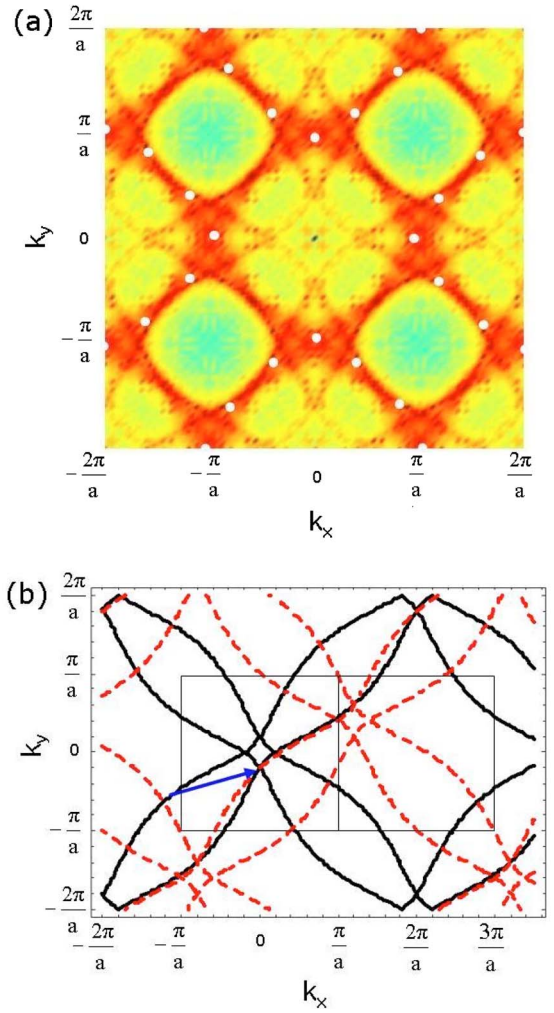

FIG. 4. (Color online) (a) Generalized susceptibility $\chi(q)$ on a color scale for the model shown in Fig. 3 for E_F=3.1 eV (red =high; green=low). Values of q are shown from $-a^*$ to a^*. The observed lattice-modulation vectors for $LaTe_{1.95}$ are shown as white spots. (b) The Fermi surface for the same band filling (solid lines), showing the CDW replica (dashed lines) translated by q_{CDW} $=(0.601a^*, 0.201a^*)$, indicated by an arrow.

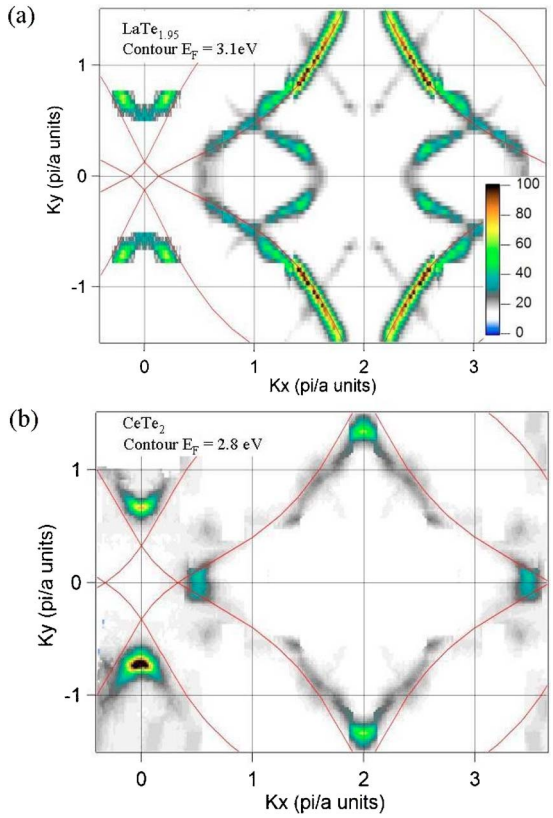

FIG. 5. (Color online) ARPES data at T=20 K showing the Fermi surface of (a) $LaTe_{1.95}$ with $h\nu$=30 eV and (b) $CeTe_2$ with $h\nu$=52 eV, obtained by integration of the electronic structure in a 100-meV window around E_F (see text). The red lines show the results of the tight-binding model described in Sec. IV for the given Fermi energies in the extended-zone scheme.

similar calculation reveals a very well-defined maximum in $\chi(q)$.[22] Since the nesting wave vector is so much better defined in RTe_3 than RTe_2, the resulting charge-density wave is also much more stable against perturbation, changing only modestly in magnitude across the entire rare-earth series.[13]

V. ARPES

Figure 5 displays Fermi surfaces of $LaTe_{1.95}$ and $CeTe_2$ measured by ARPES at photon energies of 30 and 52 eV, respectively. These maps were obtained by integration of the spectral weight between E_F-50 meV and E_F+50 meV and data were symmetrized with respect to $x=2$ and $y=0$ [except for $CeTe_2$ in the first Brillouin zone (BZ)]. We have checked that the different photon energy and data symmetrization do not change the qualitative features of these maps. Similar results were reproduced in another $LaTe_{1.95}$ sample and three other $CeTe_2$ samples.

The regions of high intensity in Fig. 5 correspond to places where Te p_x and p_y bands approach the Fermi level (either crossing it or leaving a small gap). As described in the preceding section, and also found for RTe_3,[14,15] there are two different pieces of FS, a small square centered at Γ (referred to as the inner FS) and a larger square centered at (2,0) and equivalent points that we will call the outer FS in the following discussion. The small inner square does not appear on Fig. 5 because it is entirely gapped, as will be discussed later. The outer FS is folded in the first BZ (parts of these reflections are clearly seen in $LaTe_{1.95}$), but with a weaker intensity that sometimes makes it undetectable (for details, see Ref. 14). Comparison with Fig. 3 shows that this FS is in total agreement with the simple tight-binding model based only on Te bands presented in the preceding section. In addition, we note that we do not observe a small pocket around Γ, which was predicted in some calculations to be formed by La 5d bands.[8]

In this simple tight-binding approach, the size of the outer FS is simply determined by the position of the Fermi level, i.e., the band filling. In the absence of Te deficiency, the band filling is expected to be the same for all rare-earth members of the series, as we have previously found for the tritelluride RTe_3.[22] In contrast, for the ditellurides, we find that the size of the outer FS appears significantly larger in $LaTe_{1.95}$ com-

pared to $CeTe_2$. Qualitatively, the larger outer FS in $LaTe_{1.95}$ is consistent with the presence of Te vacancies, which would increase the average number of electrons per Te (see Fig. 3). If n is the number of electrons in p_x and p_y orbitals (we assume that p_z is filled), one expects $n=3$ for stoichiometric RTe_2 from which $E_F=2.8$ eV. Quantitatively, the best fit of the data to the tight-binding model for $LaTe_{1.95}$ is indicated in Fig. 5 by the red lines, and gives $E_F=3.1$ eV± 0.1 eV, from which we obtain $n=3.1\pm 0.07$. Within an ionic picture, the finding of $n>3$ can be explained by the charge transfer from a small number of vacancies $\delta=0.1\pm 0.05$, consistent with the measured value of $\delta=0.05\pm 0.03$. In $CeTe_2$, the fitting is less accurate because a large part of the outer FS is gapped (as will be discussed later) and the intensity is concentrated at the corners, where the real data deviate from the tight-binding model (these corners are rounded by the interaction between p_x and p_y, which was neglected in the calculation).[14] Therefore, we just show the theoretical contour for $E_F=2.8$ eV, which appears correct or slightly too large, demonstrating the contrast with $LaTe_{1.95}$. This also implies that we can find the right size of FS by completely neglecting the contribution of Ce electrons, which requires a negligible coupling between Te and Ce electrons. (A significant hybridization with Ce $4f$, Ce $5d$, or Te p_z electrons would all result in a larger size of outer FS, inconsistent with our data.)

The other important information that one can extract from the ARPES data is the size and location of the CDW gap. A lower intensity on the FS map is usually correlated with a gap opening, which partially or totally removes the bands from the integration window around E_F. However, it is necessary to check simultaneously the gap opening on a map of the measurement of the full electronic structure as a function of energy, because ARPES intensity is modulated by matrix-element effects that can introduce extrinsic intensity variations. For example, the intensity appears stronger for both maps in the upper part of the outer FS ($k_y>0.5$), but this is a change of the whole band intensity; the band dispersion and shape at E_F remain the same. Similarly, the intensities at the different corners of the $CeTe_2$ map are slightly different, but they all correspond to Fermi-level crossings of bands with different absolute intensities.

As already mentioned, the small inner Fermi surface centered at the Γ point is not visible in either map, and inspection of the full electronic structure reveals a very large gap in both cases with $E_g=600$ meV, nearly two times larger than in RTe_3, indicating a very strong coupling for the CDW. Another similarity between the two maps is their fourfold symmetry (except for the extrinsic changes in intensity already discussed). This is at variance with RTe_3, for which the gap opens along one direction only, giving very different FS along k_x and k_y. This could be expected from the TEM patterns presented in Sec. IV, which show coexistence of satellites in the k_x and k_y directions, contrary to those in RTe_3, which have twofold symmetries.

The intensity along the outer FS is generally much larger than in the inner square, which indicates no gap or a much smaller gap, and the distribution of this intensity is dramatically different in the two compounds. In $LaTe_{1.95}$, most of the outer part is ungapped, and a small gap $E_g=100$ meV opens only at the corners (where the intensity is reduced in the map, it is clearly visible along k_x and, for the folded FS, along k_y). The opposite is observed in $CeTe_2$, where the spectral weight is highest on the corners, with no gap, whereas in other regions there is a small gap $E_g=100$ meV. This is again at variance with RTe_3, for which the gap decreases rapidly and monotonically from its maximum value to zero.[14]

These extended regions of small or null gaps exist because of imperfect nesting of the FS, even when there is a very large CDW coupling, as is the case here. Figure 4(b) indicates a typical situation giving an approximate but not perfect nesting for a sizable part of the outer FS. This is in contrast with RTe_3 for which there is a well-defined maximum in $\chi(q)$, and consequently regions of the Fermi surface are either very well nested or very poorly nested.[22] Not surprisingly, we observe that the more complicated nesting properties of RTe_2 directly yield more complicated FS topologies that become highly sensitive to changes of the CDW structure.

In principle, the size of the gap along the FS could be calculated from the combined knowledge of the CDW wave vectors and the shape of the original FS. This becomes quite complex here, because of the coexistence of many different CDW satellites. In many regions of the outer FS of both compounds, we observe a large gap similar to the one of the square (600 meV) coexisting with intensity near the Fermi level, suggesting domains with different CDW orientations and/or a complex superstructure of the CDW. It is therefore difficult to tell how many carriers are involved in the reconstructed FS. Nevertheless, ARPES firmly establishes that the incommensurate CDW is the driving force shaping the FS and predicts that any residual metallic properties associated with the ungapped regions of the FS will be highly sensitive to the details of the CDW structure. From the larger, ungapped section of the FS in $LaTe_{1.95}$, one can anticipate better metallic properties for this compound than for $CeTe_2$, but it is necessary to rely on complementary measurements, such as heat capacity and resistivity, to characterize the nature of the electronic properties.

VI. HEAT CAPACITY

The heat capacity of $LaTe_{1.95}$ is shown in Fig. 6. That of $CeTe_2$ is dominated by the magnetic contribution at low temperatures, and has been discussed elsewhere.[12,23] For comparison, we include similar data for $LaTe_3$ in Fig. 6(a). By 300 K, the heat capacity of both compounds has risen to approximately the Dulong-Petit value of $3R$ per mol of atoms. Below 5 K, C/T vs T^2 follows a straight line for both materials, and linear fits result in estimates for the electronic contribution to the heat capacity (y-axis intercept) of $\gamma=0.3\pm 0.06$ mJ/mol K^2 for $LaTe_{1.95}$ and 1.1 ± 0.04 mJ/mol K^2 for $LaTe_3$. CDW formation in $LaTe_3$ does not gap the entire Fermi surface,[14,15] and based on the preceding estimate of γ, the ungapped regions clearly contribute a reasonable density of states, consistent with the observation of metallic resistivity for this compound.[19,24,25]

In comparison, the electronic contribution to the heat capacity in $LaTe_{1.95}$ is significantly smaller than in $LaTe_3$. The

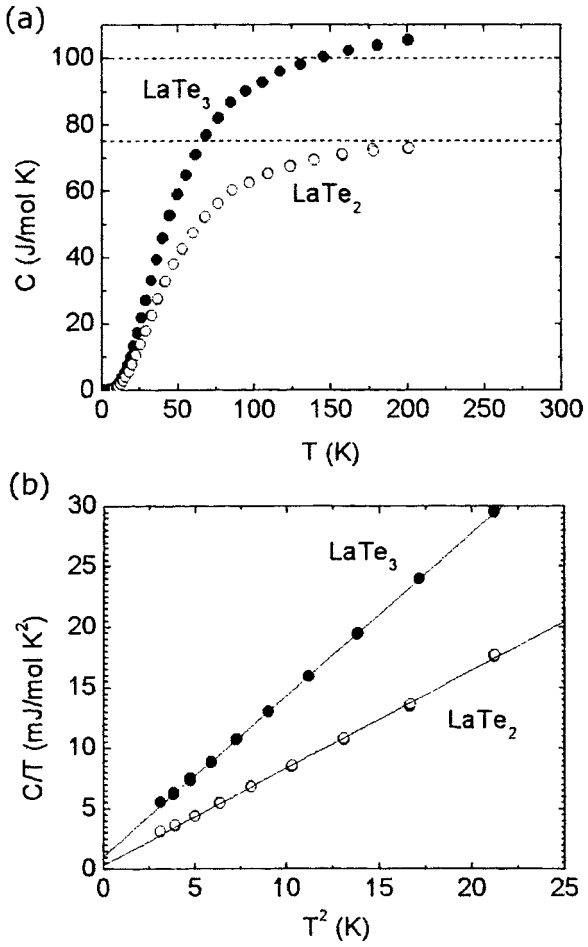

FIG. 6. (a) Heat capacity of $LaTe_{1.95}$ (open circles) and $LaTe_3$ (solid circles). Dashed lines show the Dulong-Petit limit corresponding to $3R$ per mol of atoms. (b) The same data at low temperatures shown as C/T vs T^2. Lines show the linear fit; mol refers to one formula unit.

measured value of $\gamma=0.3$ mJ/mol K^2 corresponds to a density of states (DOS) of approximately 0.13 states/eV/f.u. in a free-electron model analysis. This value is much smaller than the calculated value of 0.63 states/eV/f.u. obtained from first-principle band-structure calculation for the unmodulated structure of $LaTe_2$,[3,26] indicating that a substantial proportion of the Fermi surface has been gapped by the CDW. This picture is confirmed by electrical resistivity measurements in the following section, which show that $LaTe_{1.95}$ is far from being a good metal.

VII. RESISTIVITY

The temperature dependence of the electrical resistivity of the single-crystal $LaTe_{1.95}$ and $CeTe_2$ samples are shown in Figs. 7(a) and 7(b), respectively. The resistivity for both materials shows a strong anisotropy between the measurements in the *ab* plane (ρ_{ab}) and along the *c* axis (ρ_c), consistent with the layered crystal structure and with previous measurements.[5–7] At base temperature, we find that ρ_c/ρ_{ab} is in the range of 50 ($LaTe_{1.95}$) to 100 ($CeTe_2$). The temperature dependence of the resistivity is rather complicated, reminiscent of either a doped small-gap semiconductor or possibly a semimetal, and is certainly far from that of a good metal. Likewise, the absolute value of the resistivity at base temperature is rather high, approximately 2 mΩ cm for currents flowing in the *ab* plane. This is in contrast to the related bilayer material RTe_3, which exhibits very good metallic behavior associated with ungapped regions of the Fermi surface and a residual resistivity of only a few $\mu\Omega$ cm.[14,24,25]

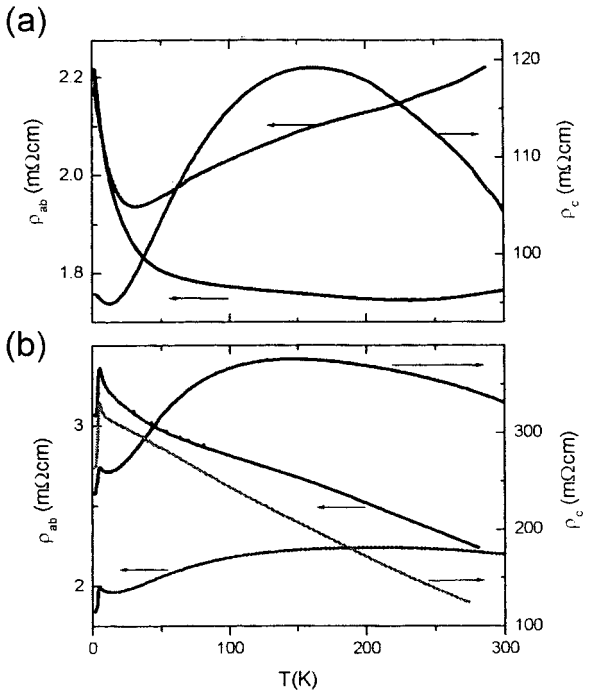

FIG. 7. Representative resistivity data for (a) $LaTe_{1.95}$ and (b) $CeTe_2$, showing ρ_{ab} (left axis) and ρ_c (right axis). Data for $LaTe_{1.95}$ were taken for crystals from the same growth batch. Data for $CeTe_2$ are shown for crystals from two different growth batches (gray and black lines; see text).

An additional feature of the resistivity of this material is that there is a sizable variation between crystals, even between samples taken from the same growth batch. For instance, the in-plane resistivity of $LaTe_{1.95}$ [Fig. 7(a), left axis] shows semiconducting behavior at low temperatures for all samples, but at higher temperatures the slope of the resistivity is more variable—two extreme cases are shown. A similar range of behavior is observed for $CeTe_2$. Representative data are shown in Fig. 7(b) for crystals taken from two different growth conditions, corresponding to initial-melt compositions of $Ce_{0.15}Te_{0.85}$ (black lines) and $Ce_{0.18}Te_{0.82}$ (gray lines). Both types of temperature dependence have been described in the published literature for this material.[5–7] This variation is presumably associated with subtle differences in Te content. Certainly our measurements imply that one should be careful reading too much into the exact temperature dependence of any one particular resistivity curve for this material. In contrast, we find that there is no sample-to-sample variation in the resistivity of RTe_3, consistent both with the absence of Te deficiency in this compound and also with the more strongly metallic nature of the material.

Finally, we note that $CeTe_2$ samples have a sharp feature in the resistivity below 6 K, which is associated with magnetic ordering of the local $4f$ electrons. Neither the temperature of this feature, nor any other thermodynamic property associated with the magnetic ordering (susceptibility or heat capacity), show any sample-to-sample variation.[22] Hence, the magnetic properties of this material appear to be rather insensitive to the exact degree of Te deficiency.

VIII. DISCUSSION

Despite considerable interest in the magnetic and electronic properties of $RTe_{2-\delta}$, few attempts have been made to determine the full crystal structure incorporating the effects of the lattice modulation. Experiments by DiMasi and coworkers, using crystals grown from an alkali-halide flux, indicated a $(2\times1\times1)$ supercell for $LaTe_2$.[1] Subsequently, Stowe, using crystals grown via chemical vapor transport, suggested $(2\times2\times1)$ and $(2\times2\times2)$ supercells for $LaTe_2$ and $CeTe_2$ respectively.[8,9] Our own experiments, using crystals grown via a self-flux, indicate that the modulation is not precisely commensurate with the lattice for either compound. These differences between crystals grown via different methods are likely real, and reflect the fact that the synthesis technique can affect both Te content and other extrinsic parameters such as strain. DiMasi has already shown that the CDW distortion is sensitive to band filling by varying the Sb content in $LaTe_{2-x}Sb_x$,[1] and our data strongly suggest that Te vacancies will also affect the CDW. Our first conclusion is therefore that the lattice modulation in $RTe_{2-\delta}$ is very sensitive to subtle extrinsic effects, including small differences in Te content or differences induced by the change in the rare-earth element.

Our model tight-binding calculation indicates that the observed modulation wave vectors in $LaTe_{1.95}$ and $CeTe_2$ can be related to nesting conditions of the Fermi surface. Calculations of $\chi(q)$ for this model Fermi surface do not show a single peak, but rather a series of broad maxima, along which the observed modulation wave vectors are found to lie. Presumably details of the real electronic structure associated with Te deficiency, strain, and the choice of rare earth will favor certain specific modulation wave vectors, consistent with the preceding conclusion.

ARPES measurements clearly show that large portions of the Fermi surface of both $LaTe_{1.95}$ and $CeTe_2$ are gapped. The maximum value of the gap is very large, around 600 meV in both cases, implying strong electron-phonon coupling. However, most regions of the FS exhibit a smaller gap of approximately 100 meV, characteristic of imperfect nesting. The position of these regions with small gaps will be very sensitive to details of the CDW, and they are consequently found to be quite different for $CeTe_2$ and $LaTe_{1.95}$, in good agreement with the different CDW structure already revealed by TEM. This situation is clearly more complex than for RTe_3, for which there is a well-defined unidirectional CDW wave vector that does not change significantly all the way across the rare-earth series.[13] Nevertheless, it is clear from this measurement that the ditellurides are not homogeneously gapped and cannot be considered as simple insulators.

How do the ungapped regions of Fermi surface contribute to the conductivity? This is not a simple question to answer, but we can make a few observations. It is clear from heat-capacity measurements that a significantly larger portion of the Fermi surface has been gapped for $LaTe_{1.95}$ than for $LaTe_3$. At first glance, this appears to contradict the ARPES data, which suggest a rather large residual FS, at least in $LaTe_{1.95}$ (in $CeTe_2$, the FS pockets are certainly very small). However, as we have explained, care must be taken in the interpretation of this FS, because we observe in our data the *coexistence* of gaps of different magnitude at the same positions in k space, so that it is not straightforward to determine how many carriers contribute to the reconstructed FS. These multiple gaps can be associated with the multiple CDW satellites observed by TEM. This situation is considerably more complex than the case of RTe_3, for which the homogeneous behavior of the CDW gap made determination of the reconstructed FS unambiguous.[14] The presence of only a very small number of carriers in the reconstructed bands near E_F would reconcile ARPES measurements with the bad metallicity observed by heat capacity and electrical conductivity. Furthermore, since there is large a distribution of small amplitude gaps, we cannot rule out the possibility that there might be on parts of the remaining FS a gap smaller than the experimental resolution (about 10 meV) that would substract yet more carriers. Given this low carrier concentration, it is understandable that resistivity data for both compounds are far from those of a good metal, in clear contrast to the tritellurides. Moreover, the CDW gap itself is substantially larger in $LaTe_{1.95}$ ($\sim$600 meV) than for $LaTe_3$ ($\sim$300 meV), implying a significant electron-phonon coupling even for the remaining ungapped regions of the FS. Finally, we note that there is substantial disorder in $LaTe_{1.95}$ arising from the Te vacancies—an effect all but absent in the stoichiometric tritelluride compound $LaTe_3$. Taken together, these observations imply that polaronic and/or localization effects may also play a significant role in substantially reducing the conductivity of this material.

IX. CONCLUSION

In summary, we have described an alternative self-flux technique to grow single crystals of $RTe_{2-\delta}$ that results in samples with very small Te deficiency (δ=0.00 and 0.05 for R=Ce and La, respectively). TEM measurements show that the lattice modulation is different for the two materials, and that in both cases it is incommensurate with the underlying lattice. The CDW distortion is different from published structures for crystals produced by different techniques, indicating that the lattice modulation is very sensitive to subtle differences caused by either varying the rare earth or changing the Te deficiency. ARPES measurements indicate that large regions of the Fermi surface are gapped for both compounds, consistent with description of the lattice modulation in terms of CDW formation driven by Fermi-surface nesting. The gap varies around the Fermi surface differently for the two compounds, reflecting the difference in lattice distortion. Heat-capacity measurements for R=La indicate that the material has a very small density of states at the Fermi level, and

resistivity measurements for both compounds show that they are far from being good metals. Given this background, it is perhaps all the more surprising to find that $CeTe_{1.82}$ superconducts under pressure.[20] Our observations show that the nesting wave vectors are somewhat poorly defined for this material, and as such, the CDW is rather sensitive to perturbation, for example, from tellurium vacancies, at least in comparison to the related tritellurides RTe_3. It remains to be seen exactly how pressure affects the electronic structure and CDW modulation of this material, but our observations suggest that the CDW will be very sensitive to such external changes. Certainly the substantial CDW gap at ambient pressure implies that there is the potential for a sizable electron-phonon coupling, a key ingredient for conventional superconductivity.

ACKNOWLEDGMENTS

We gratefully thank Robert E. Jones and A. Marshall for technical assistance with EMPA and TEM measurements and analysis. This work is supported by the DOE, Office of Basic Energy Sciences, under Contract No. DE-AC03-76SF00515. I.R.F. is also supported by the Alfred P. Sloan Foundation.

*Electronic address: irfisher@stanford.edu

[1] E. DiMasi, B. Foran, M. C. Aronson, and S. Lee, Phys. Rev. B **54**, 13587 (1996).
[2] M. H. Jung, T. Ekino, Y. S. Kwon, and T. Takabatake, Phys. Rev. B **63**, 035101 (2000).
[3] J. Laverock, S. B. Dugdale, Zs. Major, M. A. Alam, N. Ru, I. R. Fisher, G. Santi, and E. Bruno, Phys. Rev. B **71**, 085114 (2005).
[4] A. Kikichi, J. Phys. Soc. Jpn. **67**, 1308 (1998).
[5] Y. S. Kwon and B. H. Min, Physica B **281–282**, 120 (2000).
[6] B. H. Min, E. D. Moon, H. J. Im, S. O. Hong, Y. S. Kwon, D. L. Kim, and H.-C. Ri, Physica B **312–313**, 205 (2002).
[7] M.-H. Jung, B.-H. Min, Y.-S. Kwon, I. Oguro, F. Iga, T. Fujita, T. Ekino, T. Kasuya, and T. Takabatake, J. Phys. Soc. Jpn. **69**, 937 (2000).
[8] K. Stowe, J. Solid State Chem. **149**, 155 (2000).
[9] K. Stowe, J. Alloys Compd. **307**, 101 (2000).
[10] J.-S. Kang, C. G. Olson, Y. S. Kwon, S. W. Han, K. H. Kim, A. Sekiyama, S. Kasai, S. Suga, and B. I. Min, J. Phys.: Condens. Matter **16**, 9163 (2004).
[11] B. H. Min, H. Y. Choi, and Y. S. Kwon, Physica B **312–313**, 203 (2002).
[12] M. H. Jung, K. Umeo, T. Fujita, and T. Takabatake, Phys. Rev. B **62**, 11609 (2000).
[13] E. DiMasi, M. C. Aronson, J. F. Mansfield, B. Foran, and S. Lee, Phys. Rev. B **52**, 14516 (1995).
[14] V. Brouet, W. L. Yang, X. J. Zhou, Z. Hussain, N. Ru, K. Y. Shin, I. R. Fisher, and Z. X. Shen, Phys. Rev. Lett. **93**, 126405 (2004).
[15] G.-H. Gweon, J. D. Denlinger, J. A. Clack, J. W. Allen, C. G. Olson, E. D. DiMasi, M. C. Aronson, B. Foran, and S. Lee, Phys. Rev. Lett. **81**, 886 (1998).
[16] T. B. Massalski, ed., *Binary Alloy Phase Diagrams* (ASM International, Materials Park, Ohio, 1996).
[17] B. Foran, S. Lee, and M. C. Aronson, Chem. Mater. **5**, 974 (1993).
[18] S. M. Park, S. J. Park, and S. J. Kim, J. Solid State Chem. **140**, 300 (1998).
[19] N. Ru and I. R. Fisher (unpublished).
[20] M. H. Jung, A. Alsmadi, H. C. Kim, Y. Bang, K. H. Ahn, K. Umeo, A. H. Lacerda, H. Nakotte, H. C. Ri, and T. Takabatake, Phys. Rev. B **67**, 212504 (2003).
[21] J. H. Shim, J.-S. Kang, and B. I. Min, Phys. Rev. Lett. **93**, 156406 (2004).
[22] K. Y. Shin, N. Ru, V. Brouet, and I. R. Fisher (unpublished).
[23] B. H. Min, J. H. Cho, H. J. Lee, C. W. Han, D. L. Kim, and Y. S. Kwon, Physica B **281–282**, 118 (2000).
[24] E. DiMasi, B. Foran, M. C. Aronson, and S. Lee, Chem. Mater. **6**, 1867 (1994).
[25] Y. Iyeiri, T. Okumura, C. Michioka, and K. Suzuki, Phys. Rev. B **67**, 144417 (2003).
[26] S. B. Dugdale (private communication).